Optimizing a Formation-of-Arrays Mega-Antenna for High-Throughput Satellite Communications

Francesco Greco, Giacomo Bacci and Marco Luise
Dipartimento di Ingegneria dell'Informazione, University of Pisa, Pisa, Italy
email: giacomo.bacci@unipi.it

***Abstract*—This paper investigates the optimization of a mega-antenna (MEGAN) system in a geostationary orbit to provide 5G-like services through a formation of closely spaced satellites. Each satellite in the formation carries a direct radiating antenna, coordinated by a central reference satellite to create a selective multibeam radiation pattern. This paper, which elaborates on previous works on system simulations for network throughput, introduces a more efficient methodology by using an analytical approach to compute the signal-to-interference-plus-noise ratio at each coverage point. This method enables direct calculation of network efficiency in terms of available bit-rate per unit area, offering more accurate and computationally efficient optimization of the MEGAN configuration.**

***Index Terms*—Satellite communications, formation of arrays, mega-constellations, nonterrestrial network integration.**

I. Introduction and motivation

Over the last ten years, communications satellites have increasingly depended on advanced antenna systems, both in large geostationary Earth orbit (GEO) satellites and smaller low Earth orbit (LEO) satellites within mega-constellations. Looking ahead, research in non-terrestrial network (NTN) integration is focusing on coordinated formations [1] or swarms of simple satellites [2], [3] to develop a massive, virtual, distributed mega-antenna (MEGAN) in space. This architecture is structured as a formation of arrays (FoA), that is, each satellite carries a direct radiating antenna (DRA) that is driven in strict coordination with the others in the MEGAN system by a central, reference, satellite, so as to create a very selective multibeam radiation pattern on the ground. Issues related to optimization of the FoA configuration have also been tackled [4], as well as the possibility to use the MEGAN to create a satellite (cell-free) massive MIMO (mMIMO) network from GEO orbit [5]–[7].

Optimizing the FoA-based MEGAN is a complicated issue: on one side, the number of parameters involved in the problem is high (geometry of the FoA, DRA type and location, power allocation across the satellites, etc.). On the other, derivation of the key performance indicator (KPI) of the network is exceedingly time-consuming. The methodology adopted in [1], [4] is building up a MATLAB-based realistic system simulation to derive the overall network throughput in a given physical bandwidth, and the corresponding per-user throughput. Deriving such parameters is extremely time-consuming, so that optimization of FoA is also carried out with a number of heuristics, and the optimization space is not thoroughly investigated.

This work was supported by the Italian Ministry of Education and Research (MUR) in the framework of the FoReLab Project (Department of Excellence), as well as by the European Union under the Italian National Recovery and Resilience Plan (NRRP) of NextGenerationEU, partnership on "Telecommunications of the Future" (PE00000001 – Program "RESTART").

In this paper, we started form the same basic system architecture as in [1], [4], but we adopt a different KPI based on the analytic accurate computation of the signal-to-interference-plus-noise ratio (SINR) at every point of the coverage area on Earth, and, from that, the evaluation of the *area efficiency* of the network in terms of bitrate/km^2 at Shannon capacity. From this KPI, deriving network throughput and user bitrate is immediate: this approach turns out to be sufficiently accurate to capture network performance, as well as more computationally efficient, so that optimization of the FoA MEGAN configuration can explore new directions not previously covered.

After this introduction, we describe the FoA system setup in Sect. II, and we introduce the procedure to derive the network KPI in Sect. III. Sect. IV illustrates our numerical results, and the conclusion is finally reported in Sect. V.

II. System and Network model

In general, a FoA consists of an arbitrary configuration of S satellites, each equipped with a custom array of N radiating elements. As illustrated in [1, Fig. 1], we consider a planar arrangement in the yz-plane, in which the position of the n-th radiating element within the array hosted by the s-th satellite, relative to the origin of the reference system, is denoted as $\mathbf{u}_s(n) \in \mathbb{R}^3$, where $n = 1, \dots, N$ and $s = 1, \dots, S$. This position can be expressed hierarchically as $\mathbf{u}_s(n) = \mathbf{r}_s + \mathbf{r}_n$, where $\mathbf{r}_s = [0, y_s, z_s]^T$ represents the location of the s-th array's center within the formation, and $\mathbf{r}_n = [0, y_n, z_n]^T$ denotes the relative position of the n-th radiating element with respect to its array center. The *array response vector* $\mathbf{a}_s(\varphi, \theta) \in \mathbb{C}^N$ for the s-th satellite, corresponding to a plane wave with wavelength λ incident at an azimuth angle φ and an elevation angle θ, is given by

$$\mathbf{a}_s(\varphi, \theta) = g(\theta) \left[e^{\mathrm{j}\mathbf{k}^T(\varphi,\theta)\mathbf{u}_s(1)}, \dots \, e^{\mathrm{j}\mathbf{k}^T(\varphi,\theta)\mathbf{u}_s(N)} \right]^T \quad (1)$$

where $g(\theta)$ is the array element radiation pattern, and

$$\mathbf{k}(\varphi, \theta) = \frac{2\pi}{\lambda} \left[\cos\theta \cos\varphi, \ \cos\theta \sin\varphi, \ \sin\theta \right]^T \quad (2)$$

is the wave vector. To better focus on the impact of the FoA geometry, in this paper we assume $g(\theta) = 1$. To include

its effect, e.g., using the circular-symmetric direct radiating antenna model, please refer to [1, Sect. II].

The *global* array response vector of the FoA is

$$\mathbf{a}(\varphi,\theta) = \left[\mathbf{a}_1^T(\varphi,\theta),\ldots,\mathbf{a}_S^T(\varphi,\theta)\right]^T \tag{3}$$

which depends on the geometry of both the S satellites within the FoA, and the N radiating elements within each satellite.

In this paper, we focus on two different geometries for both satellites and radiating elements: uniform planar array (UPA) and circular uniform concentric array (CUCA). For a more compact notation, both satellite s and radiating element n are identified by a generic element with index $m \in \{n, s\}$. In the UPA configuration, which corresponds to the example illustrated in Fig. 1a with $M = 49$, the elements are regularly spaced at the same interval Δ_m along both axes (Δ_N for the radiating elements, and Δ_S for the satellites):

$$\begin{aligned} y_m &= \Delta_m \left(-\frac{\sqrt{M}-1}{2} + |m-1|_{\sqrt{M}} \right) \\ z_m &= \Delta_m \left(-\frac{\sqrt{M}-1}{2} + \left\lfloor \frac{m-1}{\sqrt{M}} \right\rfloor \right) \end{aligned} \tag{4}$$

where $M \in \{N, S\}$ is the number of elements, $|a|_b = a \mod b$, and $\lfloor a \rfloor$ denotes the floor function. Note that, based on the UPA symmetry, M is a square integer number.

In the CUCA configuration, the element locations are based on a numerical algorithm, that works as follows (further details are not reported for the sake of brevity): given a desired array size M and a distance Δ_m, it derives the arrangement (with the closest size to M) in which the elements are placed on concentric circles, such that Δ_m is fulfilled both within each circle, and across adjacent circles. An example with $M = 47$ is illustrated in Fig. 1b, in which the axes are normalized with respect to Δ_m. Empirically, the array size provided by the algorithm gets closer to the desired M as M increases, as are the typical cases considered in the numerical results of Sect. IV. For a fair comparison, we will select values for S and N for both configurations which yield around the same number of total elements $N \times S$. Note also that alternative arrangements are possible, such as the ones considered in [5]: the assessment of such configurations is left for future work.

To evaluate the impact of the FoA geometry (which includes both satellites' and radiating elements' locations), we can compute the antenna array pattern

$$\zeta(\theta,\varphi) = \left| \frac{1}{\sqrt{NS}} \mathbf{a}^H(0,0)\mathbf{a}(\varphi,\theta) \right|^2 \tag{5}$$

of the reference beam, i.e., the normalized received power density radiated by the FoA in the generic direction (φ, θ) when it is aimed at $\varphi = \theta = 0$. Fig. 2 illustrates the array pattern (5) of a FoA using the UPA configuration for both satellites and radiating elements, with $S = 25$, $N = 9$, $\Delta_\mathsf{N} = 4.5\lambda$, and $\Delta_\mathsf{S} = 2L$, where $\lambda \approxeq 13.6\,\mathrm{cm}$ is the wavelength at carrier frequency $2.2\,\mathrm{GHz}$, and $L = (\sqrt{N}-1)\Delta_\mathsf{N} = 9\lambda = \approxeq 1.23\,\mathrm{m}$ is the satellite side length (the selected azimuth angles

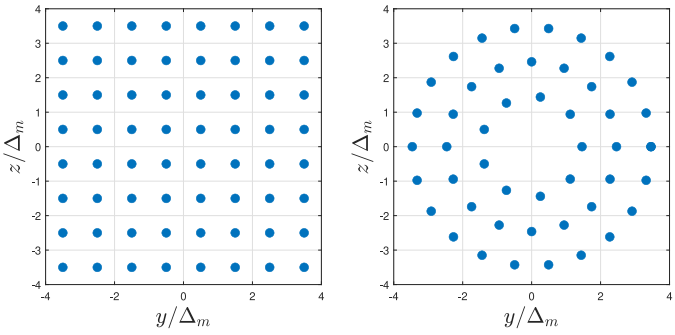

(a) $M = 49$. (b) $M = 47$.

Fig. 1: Examples of (a) UPA and (b) CUCA geometries.

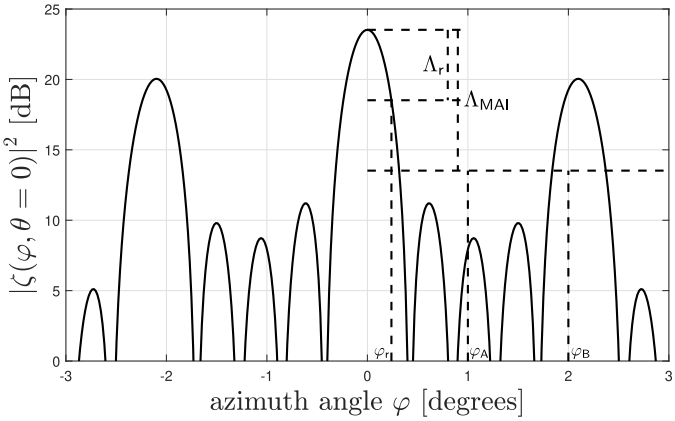

Fig. 2: FoA array response (UPA for both FoA and satellite arrays, $S = 25$, $N = 9$, $\Delta_\mathsf{S} \approxeq 2.46\,\mathrm{m}$, $\Delta_\mathsf{N} \approxeq 0.61\,\mathrm{cm}$).

and the quantities Λ_r and Λ_MAI will be defined in Sect. III-B). Please refer to [1], [4] for further considerations on the impact of the system parameters on the array pattern.

The FoA , combined with appropriate beamforming techniques, enables the creation of a tightly focused multibeam footprint on Earth, enabling connectivity for mobile users equipped with handheld terminals. In this work, we employ a straightforward beamforming approach to generate a regular beam pattern (for alternative methods, including precoding and radio resource management (RRM) techniques, please refer to [5], [8]). Specifically, we consider a multibeam satellite network utilizing frequency reuse to ensure continuous spatial service coverage within a target area of radius R. Each beam serves a set of user terminals (UTs) using an unspecified multiplexing scheme based on orthogonal resources in time, frequency, or both. Adopting a conventional frequency-reuse scheme with a reuse factor of K [9], all beams continuously transmit with a proportionally reduced bandwidth, leading to a corresponding reduction in the aggregate bitrate per beam by a factor of K. Additionally, we assume that the downlink operates in the S-band with a total available bandwidth of B [10]. This frequency band, located adjacent to terrestrial mobile network allocations, facilitates the reuse of terrestrial UT antennas and radio frequency (RF) front-end components.

III. Methodology

A. Identification of the main KPIs

In order to measure the performance of the system introduced in Sect. II in a fair and technology-agnostic manner, we focus on the Shannon-Hartley capacity $\mathcal{C}$ to compute the main KPI, represented by the *area throughput* ρ (to be defined later on). We thus focus first on evaluating [9]

$$\mathcal{C} = \frac{1}{2}\log_2\left(1+\frac{P_S}{P_N+P_I}\right) = \frac{1}{2}\log_2\left(1+\frac{1}{\gamma^{-1}+\mu^{-1}}\right) \tag{6}$$

where the factor $1/2$ follows from using all quantities at RF,

$$P_S = \iint_{(\varphi,\theta)\in\mathcal{A}_{\mathsf{ref}}} |\zeta(\varphi,\theta)|^2 \, d\theta d\varphi \tag{7}$$

is the useful power measured in the reference beam $\mathcal{A}_{\mathsf{ref}}$, which covers an area denoted with A_{ref}, whereas $P_N = N_0 B/K$ and P_I correspond to the noise and the interference powers, respectively, where N_0 is the additive white Gaussian noise (AWGN) power spectral density (PSD), and B/K is the allocated bandwidth per color (and hence K times lower than the system total bandwidth B). As a consequence, $\gamma = P_S/P_N$ and $\mu = P_S/P_I$ denote the signal-to-noise ratio (SNR) and the signal-to-interference ratio (SIR) values, respectively.

Conventionally, we assume the reference beam to be the one located in the center of the coverage area and identified by index 0 (hence, with its center at $\varphi_0 = \theta_0 = 0$). This choice is due to investigating the worst-case scenario, as the center beam suffers from the interferences from all surrounding beams. Based on this assumption, we can compute P_I as

$$P_I = \sum_{i\in\mathcal{I}} \iint_{(\varphi,\theta)\in\mathcal{A}_{\mathsf{ref}}} |\zeta(\varphi-\varphi_i,\theta-\theta_i)|^2 \, d\theta d\varphi \tag{8}$$

where θ_i and φ_i denote the elevation and the azimuth angles of the ith beam, respectively, and $\mathcal{I}$ is the set of interfering beams. Note that (8) follows from the fact that the array pattern covering each beam is simply a shifted version (in the space domain) of the one pointing towards the reference beam.

Using (6), we can compute the area throughput ρ as follows:

$$\rho = \frac{\mathcal{C}}{A_{\mathsf{ref}}} \cdot \frac{B}{K} \qquad \left[\frac{\text{bit/s}}{\text{km}^2}\right] \tag{9}$$

which provides an effective metrics to evaluate the performance of the system, to be possibly compared with that achieved by other technologies, such as the terrestrial ones.

B. Performance evaluation setup

The network model introduced in Sect. II represents a convenient way to illustrate how the resources (notably, the bandwidth) are distributed across the different beams, as if the array radiation pattern was clearly separated across the beams. However, as can be noted from (5), it has a continuous behavior, and a significant amount of the power falls on adjacent beams, thus generating the multiple access interference (MAI) formulated as in (8). The most relevant contribution is due to the presence of the grating lobes, which occur from the combined effect of the array and FoA patterns, and in particular due to the distance across the satellites, which makes the resulting FoA MEGAN irregularly spaced.

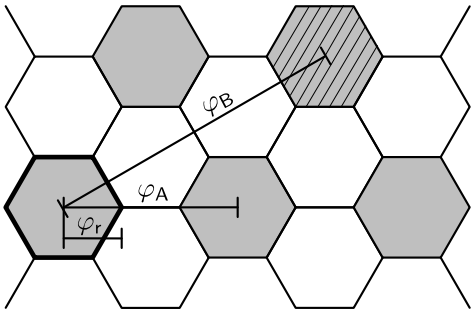

Fig. 3: Beam placement, used to compute the location of interfering beams $\mathcal{I}$ based on the FoA array response.

To evaluate both (7) and (8), and eventually (9), with sufficiently high accuracy while achieving scalability of the system and maintaining a computational time, we adopt the following approach:

- we first compute (5) with a medium-resolution grid of θ and φ, i.e, with spacing δ^{M}, in order to evaluate the beam radius r, based on a threshold Λ_{r} with respect to the maximum value achieved in $\theta = \varphi = 0$;
- by combining the radius r and the reuse factor K over the maximum satellite coverage area (with radius R), we identify the location of the potential interfering beams, and we select the ones $\mathcal{I}$, with coordinates (φ_i, θ_i), which host grating lobes whose amplitude is larger than a threshold Λ_{MAI} with respect to the maximum value achieved in $\varphi = \theta = 0$;
- we then compute (5) with a high-resolution grid of θ and φ, i.e., with spacing δ^{H}, centered around the locations of the reference beam, with coordinates $(\theta_0 = 0, \varphi_0 = 0)$, and of the main interfering beams (with coordinates (θ_i, φ_i), with $i = 1, \ldots, |\mathcal{I}|$).

For the sake of clarity, Fig. 3 illustrates the method described above with the reduced-scale system (illustrated in [1, Fig. 1]), whose array pattern is shown in Fig. 2. Using $\Lambda_{\mathsf{r}} = -5\,\text{dB}$, we obtain $\varphi_{\mathsf{r}} \cong 0.24°$, which provides $r = h\tan\varphi_{\mathsf{r}}$, where h is the satellite orbital height (for simplicity, here we derive the radius considering only one dimension, φ, assuming circular symmetry; in the numerical results provided in Sect. IV, we evaluate (5) over the 2D plane, thus considering the effect of both θ and φ). Using a reuse factor $K = 3$, we can build the beam locations provided in Fig. 3, in which the reference beam is identified by the thick edges, and the gray-shaded hexagons represent the potential interfering beams. Let us consider the two beams locates on the right-hand side with respect to the reference beam. The one with azimuth φ_{A}, albeit closer to the reference beam, shows a pattern whose amplitude is below the threshold $\Lambda_{\mathsf{MAI}} = -10\,\text{dB}$ (see Fig. 2), whereas the one with azimuth φ_{B} provides $|\zeta(\varphi_{\mathsf{B}}, 0| \geq \Lambda_{\mathsf{MAI}}|\zeta(0,0)|$. Thanks to the pattern reciprocity, the latter is included in the set $\mathcal{I}$ (and hence reported with the diagonal pattern in Fig. 3),

parameter	*Value*
carrier frequency f_0	2.2 GHz
carrier wavelength λ	13.64 cm
orbital height h	35,786 km
satellite coverage radius R	1,000 km
service bandwidth B	60 MHz
reuse factor K	3
number of satellites S	225 (UPA), 224 (CUCA)
number of array elements N	49 (UPA), 47 (CUCA)
array element spacing Δ_{N}	4.5λ
MAI threshold Λ_{MAI}	-20 dB
SNR γ	12 dB
medium-resolution grid spacing δ^{M}	3×10^{-3} deg
high-resolution grid spacing δ^{H}	2.15×10^{-5} deg

Table I: Main system parameters.

whereas the former does not contribute to the MAI (8).

For a given network configuration (which includes the FoA parameters introduced in Sect. II), we can thus derive the parameters r and (φ_i, θ_i), $i = 1, \ldots, |\mathcal{I}|$, based on the method illustrated above, and thus numerically evaluate (9), using the reciprocity of the array pattern across reference beam and interfering beams, and where $A_{\mathsf{ref}} = 3\sqrt{3}r^2/2$, assuming beams with hexagonal shape. This analysis is conducted in the following section, for a selection of different configurations and use cases.

IV. Numerical results

Unless otherwise specified, the results reported in this section make use of the parameters reported in Table I, assuming a GEO configuration.

A. Beam radius

To investigate the performance of the different configurations, we evaluate the impact of the threshold Λ_{r}, which determines the beam radius, and hence the positions of the beams in the network (with impact on the location of the interfering beams $\mathcal{I}$). For this analysis, we consider $\Delta_{\mathsf{S}} = 10$ m. Fig. 4 shows both the area capacity ρ (blue lines, left axis) and the beam radius r (red lines, right axis) as functions of Λ_{r}, for UPA and CUCA configurations, applied to both FoA and satellite array configurations. As an example, solid lines with square markers depict the results for a CUCA FoA with UPA-based satellites. As can be seen, the measured behavior clearly identifies an optimal threshold, $\Lambda_{\mathsf{r}}^{\star} = -1.72$ dB for all configurations: smaller thresholds force interfering beams to be placed too close to each other, whereas larger thresholds are too conservative, with a negative impact on the area throughput ρ. As a consequence, in the remainder of the section we will consider this threshold to compute the beam radius r.

B. Distance between satellites

Since, as observed in all multiple-access networks, such as the terrestrial cellular networks [9], and confirmed by [1], the system under investigation is *interference-limited*, it is important to study the behavior of the KPIs detailed in Sect. III-A as a function of the FoA parameters. In particular, we are interested in determining the optimal inter-satellite

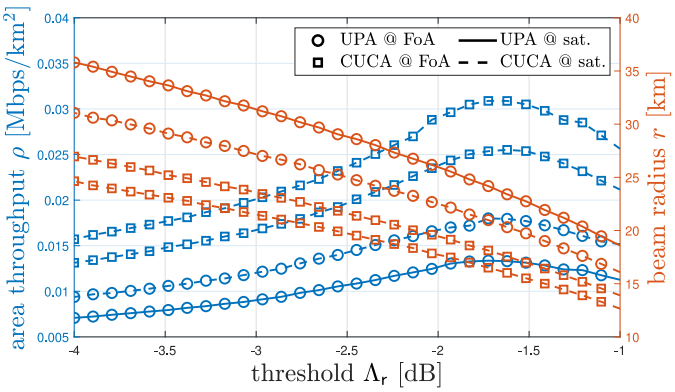

Fig. 4: Area throughput and beam radius as functions of Λ_{r}: the optimal threshold is -1.72 dB for all combinations.

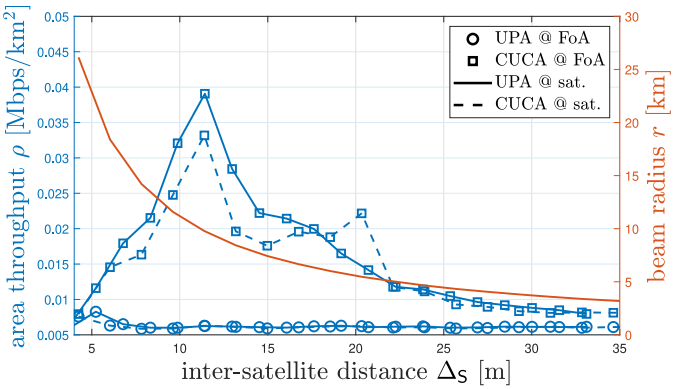

Fig. 5: Area throughput and beam radius as functions of the inter-satellite distance: the best combination is achieved by a CUCA FoA with UPA-based satellites, spaced 11.5 m apart.

distance Δ_{S} that yields the maximum area throughput ρ. Fig. 5 reports the area capacity ρ (blue lines, left axis) as a function of Δ_{S}, for UPA and CUCA configurations for both FoA and satellite array configurations. Fig. 5 also reports the beam radius r (red line, right axis). Since all four configurations yield approximately the same radius, only one line is reported for the reader's convenience, also confirming the fairness of the comparison. The numerical results confirm the findings of [1]: increasing Δ_{S} increases the directivity of the FoA pattern, with a beneficial impact on ρ; however, after a certain inter-satellite distance (11.5 m), this positive effect is counter-compensated by dominant grating lobes, which raise the MAI and thus steeply reduce ρ. Two interesting observations can be drawn: *i*) unlike [1], which adopts an approach based on a minimum SINR specified by [11], the obtained values for ρ are higher, since they are based on the maximum achievable $\mathcal{C}$ (6); *ii*) the best configuration is provided by a CUCA-based FoA equipped with UPA satellite arrays.

C. Tapering techniques

To further control the shape of the array pattern, with special emphasis on keeping the grating lobes as low as possible,

which are the responsible of MAI, and in turn of low performance in terms of ρ, we can apply *tapering* techniques [12]. This consists in applying different weights to feed the DRAs of each satellite, according to specific windowing (power) profiles $\mathbf{w} = \{w_s\}_{s=1}^{S}$, with $0 \leq w_s \leq 1$. This means that the FoA response vector becomes the one reported in (3), in which each element $\mathbf{a}_s(\varphi, \theta)$ is scaled by w_s:

$$\mathbf{a}(\varphi, \theta) = \left[w_1 \cdot \mathbf{a}_1^T(\varphi, \theta), \ldots, w_S \cdot \mathbf{a}_S^T(\varphi, \theta)\right]^T \qquad (10)$$

Note that (10) coincides with (3) in case $w_s = 1$ for all $s = 1, \ldots, S$. This is equivalent, in the space domain, to the convolution of the array response with a cardinal sine, which is responsible of the grating lobes observed in Fig. 2, and which become more and more important as Δ_S increases [1]. To better focus the array pattern towards the reference beam while reducing the out-of-beam emissions, we can resort to consolidated windowing techniques available in the literature. In this work, we make use of the 1D Kaiser-Bessel (KB) and Dolph-Chebyshev (DC) windows [12], that are extended to the 2D array structure as follows:

- for UPA FoA geometries, we consider the 1D window $\tilde{\mathbf{w}} = \{\tilde{w_m}\}_{m=1}^{\sqrt{S}}$, with length $\sqrt{S}$, and we obtain the 2D weights as $w_s = \tilde{w}_y \cdot \tilde{w}_z$, where $y = -(\sqrt{S}-1)/2 + |s-1|_{\sqrt{S}}$ and $z = -(\sqrt{S}-1)/2 + \lfloor (s-1)/\sqrt{S} \rfloor$;
- for CUCA FoA geometries, we consider the one-sided 1D window $\tilde{\mathbf{w}} = \{\tilde{w}_c\}_{c=1}^{C}$, with C denoting the number of concentric circles of the FoA configuration (e.g., 3 in the example of Fig. 1b), and we obtain the 2D weights as $w_s = \tilde{w}_c$, where c is the circle index the satellite s belongs to (with $c = 1$ and $c = C$ denoting the inner and the outer circles, respectively).

Fig. 6 shows both the area capacity ρ (blue lines, left axis) and the beam radius r (red lines, right axis) as functions of Δ_S, using the 1D KB window with parameter $\beta = 8$ and the 1D DC window with side-lobe level (SLL) $-20\,\mathrm{dB}$ (these parameters are selected based on a numerical exhaustive search). The satellite arrays are UPA-based, whereas both UPA and CUCA FoA configurations are considered. As can be seen by comparing the results with Fig. 5, the KB-based tapering yields worse performance compared to the ones achieved without tapering, whereas the DC approach significantly boosts the system performance: with an UPA-based FoA, ρ is roughly 10 times the one achieved without tapering, while we can observe a twice increase when considering the CUCA-based FoA. However, note that alternative implementations of the 2D mapping of the 1D windows may provide additional improvements (especially in the case of KB tapering).

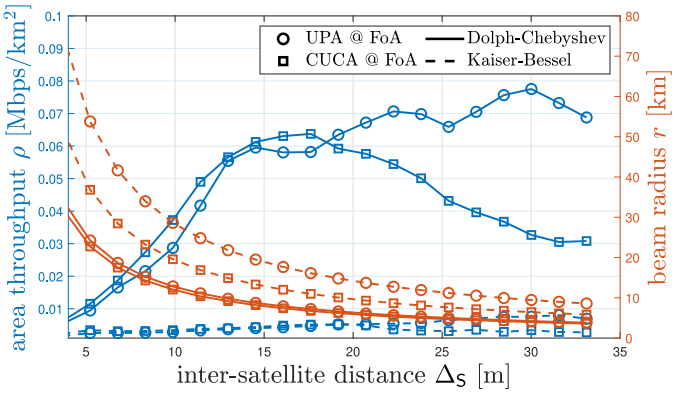

Fig. 6: Area throughput and beam radius as functions of Δ_S with tapering: the best combination is given by UPA configurations at both FoA and satellites, using DC tapering.

V. Conclusions and Perspectives

This paper investigated the impact of system parameters of a FoA-based MEGAN for high-throughput satellite communications, using the area throughput, expressed as the ratio between the Shannon capacity and the beam coverage. The results of our exhaustive numerical search show that the best configuration is a circular FoA with conventional, square DRAs on board each satellite. A further relevant optimization factor is represented by *power tapering* from the center to the edge of the FoA, in particular via Dolph-Chebyshev windowing. The approach proposed in this paper can be extended to a number of different configurations, including: LEO orbits, additional geometries for both FoA and satellite arrays, precoding and RRM-based beamforming techniques, more detailed fading models, also considering machine learning techniques to further compute and predict optimal parameter selections.

References

[1] G. Bacci, R. De Gaudenzi, M. Luise, L. Sanguinetti, and E. Sebastiani, "Formation-of-arrays (FoA) antenna technology for high-throughput mobile non terrestrial networks," *IEEE Trans. Aerosp. Electron. Syst.*, vol. 59, no. 5, pp. 4919–4935, 2023.

[2] D. Tuzi, T. Delamotte, and A. Knopp, "Satellite swarm-based antenna arrays for 6G direct-to-cell connectivity," *IEEE Access*, vol. 11, pp. 36 907–36 928, 2023.

[3] R. Deng, B. Di, and L. Son, "Ultra-dense LEO satellite based formation flying," *IEEE Trans. Commun.*, vol. 69, no. 5, pp. 3091–3105, 2021.

[4] G. Bacci, R. De Gaudenzi, M. Luise, E. Sebastiani, P. Angeletti, and J. R. González, "Optimizing a formation-of-arrays (FoA) satellite antenna system for very-high-throughput communications," *IEEE Trans. Aerosp. Electron. Syst.*, vol. 60, no. 3, pp. 3348–3367, 2024.

[5] R. De Gaudenzi, G. Bacci, M. Luise, L. Sanguinetti, and P. Angeletti, "Applicability of CF-MIMO precoding to a formation of arrays (FoA) for mobile satellite communications," *IEEE Trans. Aerosp. Electron. Syst.*, 2025, under review.

[6] M. Y. Abdelsadek, G. K. Kurt, and H. Yanikomeroglu, "Distributed massive MIMO for LEO satellite networks," *IEEE Open J. Commun. Soc.*, vol. 3, pp. 2162–2177, 2022.

[7] A. Guidotti, A. Vanelli-Coralli, and C. Amatetti, "Federated cell-free MIMO in nonterrestrial networks: Architectures and performance," *IEEE Trans. Aerosp. Electron. Syst.*, vol. 60, no. 3, pp. 3319–3347, 2024.

[8] P. Angeletti and R. De Gaudenzi, "Heuristic radio resource management for massive MIMO in satellite broadband communication networks," *IEEE Access*, vol. 9, pp. 147 164 – 147 190, 2021.

[9] T. S. Rappaport, *Wireless Communications: Principles and Practice*. London, England: Pearson Education, 2014.

[10] "On the harmonised use of radio spectrum in the 2 GHz frequency bands for the implementation of systems providing mobile satellite services," Official Journal of the European Union, Tech. Rep. 2007/98/EC, 2007.

[11] "Technical specification group radio access network; solutions for NR to support non-terrestrial networks (NTN) (Release 16," 3rd Generation Partnership Project (3GPP), Tech. Rep. Technical Specification TS 38.821 V16.2.0, 2023.

[12] B. Porat, *A Course in Digital Signal Processing*. Hoboken, NJ: Wiley, 1996.